REPORT DOCUMENTATION PAGE

Form Approved OMB No. 0704-0188

1. REPORT DATE *(DD-MM-YYYY)*	2. REPORT TYPE	3. DATES COVERED *(From – To)*
05-08-2009	Final Report	16 Jul 09 - 02-Feb-10

4. TITLE AND SUBTITLE

Experimental Validation of an Aeroelastically Scaled Sensorcraft Model

5a. CONTRACT NUMBER
FA8655-07-1-3111

5b. GRANT NUMBER

5c. PROGRAM ELEMENT NUMBER

6. AUTHOR(S)

Professor Jonathan E Cooper

5d. PROJECT NUMBER

5d. TASK NUMBER

5e. WORK UNIT NUMBER

7. PERFORMING ORGANIZATION NAME(S) AND ADDRESS(ES)

University of Liverpool
Brownlow Hill
Liverpool L693BX
United Kingdom

8. PERFORMING ORGANIZATION REPORT NUMBER

N/A

9. SPONSORING/MONITORING AGENCY NAME(S) AND ADDRESS(ES)

EOARD
Unit 4515 BOX 14
APO AE 09421

10. SPONSOR/MONITOR'S ACRONYM(S)

11. SPONSOR/MONITOR'S REPORT NUMBER(S)
Grant 07-3111

12. DISTRIBUTION/AVAILABILITY STATEMENT

Approved for public release; distribution is unlimited.

13. SUPPLEMENTARY NOTES

14. ABSTRACT

This report results from a contract tasking University of Liverpool as follows: 1.Development of a scaled Finite Element model of the wind tunnel model
2.Design and manufacture of wind tunnel model of a half-span sensorcraft with load alleviation device on the outer section of the wing Static and dynamic laboratory tests
3.Static tests to investigate non-linear deflection behaviour (with AFIT)
4.Static and dynamic wind tunnel tests to investigate performance of gust load alleviation device
5.Comparison between numerical predictions and experimental tests
6.Interim and final reporting

15. SUBJECT TERMS

EOARD, Structural Dynamics, Aerodyanamics, Aeroelasticity

16. SECURITY CLASSIFICATION OF:			17. LIMITATION OF ABSTRACT	18, NUMBER OF PAGES	19a. NAME OF RESPONSIBLE PERSON
a. REPORT	b. ABSTRACT	c. THIS PAGE			SURYA SURAMPUDI
UNCLAS	UNCLAS	UNCLAS	UL	27	19b. TELEPHONE NUMBER *(Include area code)* +44 (0)1895 616021

Experimental Validation of an Aeroelastically Scaled Sensorcraft Model

FINAL REPORT

16th July 2009

EOARD Contract FA 8655-07-1-3111

Professor J. E. Cooper.
Dept of Engineering
University of Liverpool

SUMMARY

This report describes the work undertaken in a programme aiming to design, manufacture and test a passive load gust alleviation device for use on a sensorcraft structure. The development of a full scale aeroelastic model of a sensorcraft is described along with the aeroelastic scaling approach employed to develop a scaled half model that could be tested in a wind tunnel. Numerical studies demonstrating the effectiveness of the gust alleviation device are described. The design of a wind tunnel model is also discussed. A complementary project performing the design, manufacture and static testing of a scaled half sensorcraft model is described, however, unfortunately, it was not possible to use this structure for wind tunnel testing.

1. INTRODUCTION

There is much recent interest at the AFRL Air Vehicle Directorate [1-4] in the development of unmanned High Altitude Long Endurance (HALE) or Sensorcraft air vehicles that are able to provide a 360^{o} sensor coverage whilst maintaining moderate stealth characteristics. The sensor requirement has led to a re-visit of the pioneering work into joined-wing aircraft by Wolkovich [5], Kroo and Gallman [6-8] which has been recently surveyed by Livne [9].

Typical proposed joined-wing sensorcraft structural lay-outs are shown in Figure 1 and it can be deduced that the aeroelastic behaviour is likely to be very different from conventional aircraft configurations.

Figure 1. Examples of Proposed Joined Wing Sensorcraft Aircraft

Much of the work on sensorcraft has been focused upon the optimisation of the aircraft structure, aiming fora minimisation in the mass. The outer wing of the sensor craft design leads to the high aspect ratio, which is very favourable for reduction in fuel consumption and range extension. However, it produces high bending moments, particularly when encountering manoeuvres or gusts. Due to its significant flexibility there have been concerns about:

- the ability to maintain a shape that does not affect the sensor performance
- the loads that may result from gusts
- the need to use non-linear static and dynamic aeroelastic analysis in order to account for large geometric deflections.

One of the critical design cases for joined-wing designs is the buckling of the rear wing structure. Previous work [2] has shown that non-linear buckling analysis is required in order to estimate accurately the deflections and resulting loads that occur. Linear analysis for buckling under critical gusts loads significantly increases the optimized wing structural weight, almost doubling it, and when non-linear analysis is used to produce a more accurate analysis through the inclusion of geometric nonlinear stiffening effects, the wing tip deflection increases and the optimized wing weight again increases significantly.

The use of some form of gust load alleviation system is therefore very desirable, as this should lead to a significant reduction in structure, and hence weight, that is required. One possible solution is the design of active load alleviation systems using all of the control surfaces; however, such an approach is complex, requiring the avionics for such a system to be carried on the sensorcraft, and a certain amount of system redundancy must be included to allow for system failures.

Previous work funded by AFRL through the EOARD [10-11] has investigated the use of a passive gust alleviation device for the reduction of loads, and hence structural weight, on a sensorcraft aircraft. The objective of this project is to design, manufacture and test (both statically and dynamically) a half span wind tunnel model. This report describes the development of a full scale numerical aeroelastic model to provide parameters from which the aeroelastic scaling can be performed, and the scaling approach used to determine the dimensions of a scaled half wing tunnel model. A baseline FE model was developed to provide the basis for the aeroelastic scaling process and to provide dimensions for the manufacture of the wind tunnel model. A scaled half sensorcraft model was designed, manufactured and ground tested, and details of these tests are also described.

2. DEVELOPMENT OF A FULL SIZE AEROELASTIC MODEL

In order to produce a perfectly scaled aeroelastic model of the sensorcraft, the full scale FE and aerodynamic model needs to be made available. However, for this project such a model was not available, and instead the University of Liverpool was supplied with the natural frequencies, mode shapes and generalised mass and stiffnesses from a full scale FE model.

This chapter describes how an aeroelastic model of the full size sensorcraft model has been developed by adding panel method aerodynamics to supplied modal data and planform. The model was then used to obtain static and dynamic aeroelastic behaviour of the full-scale model which can then be employed in the scaling process.

2.1 Supplied Data

The aeroelastic sensorcraft model was built using the ZAERO package based on the data supplied in "Boeing_410E4- 21r2_Mode_Shapes_Reduced_Set_v04Bond.doc". Mode shape data, grid point location (101 points), inertia, generalised mass and stiffness data are used to create a modal model as input to the software package.

2.2 Aeroelastic Modelling

Given the standard aeroelastic equation in physical space y

$$\mathbf{A}\ddot{\underline{y}} + \mathbf{E}\underline{y} = q\mathbf{Q}\underline{y} \tag{1}$$

where A and E are the mass and stiffness matrices respectively, q is the dynamic pressure and Q is the aerodynamic force matrix. The system can be transformed into modal space p such that

$$\begin{aligned} \phi^T\mathbf{A}\phi\ddot{\underline{p}} + \phi^T\mathbf{E}\phi\underline{p} &= q\phi^T\mathbf{Q}\phi\underline{p} \\ \mathbf{A}_p\ddot{\underline{p}} + \mathbf{E}_p\underline{p} &= q\phi^T\mathbf{Q}\phi\underline{p} \end{aligned} \tag{2}$$

where A_p and E_p are the diagonal mass and stiffness matrices respectively. The aerodynamic matrix Q is calculated from the DLM code in the ZAERO software. This equation can be used to solve the flutter problem. For static aeroelastic analysis the equation simplifies to

$$\mathbf{E}_p\underline{p} = q\phi^T\mathbf{Q}\phi\left(\underline{p} + \underline{p}_0\right) \tag{3}$$

where p_0 is a vector of wind-off deflections, such as angle of attack.

2.3 Structural Modelling

The mass and stiffness matrices supplied correspond to a set of mass normalised matrices, giving an identity matrix for the mass and the stiffness matrix is a diagonal matrix containing the squares of the natural frequencies. Table 1 summarises the provided properties. Note that the resulting mode shapes are normalised from the true scaled mode shapes Ψ based on the relationship

$$\phi = \psi \mathbf{M}^{1/2} \tag{4}$$

where ϕ is the supplied mode shape matrix.

Mode	Natural Frequency (Hz)	Generalised Mass	Generalised Stiffness
1	0.7677478	1	23.27003
2	0.8588396	1	29.11950
3	1.211805	1	57.97290
4	1.287392	1	65.43068
5	2.193815	1	190.0027
6	2.574066	1	261.5768
7	2.903505	1	332.8166
8	3.270949	1	422.3839
9	3.310896	1	432.7638
10	4.115517	1	668.6649

Table 1 Supplied data

2.4 Aerodynamic Modelling

The aerodynamic model has to be generated using a panel method, whose grid covers the planform of the (unknown) Finite Element (FE) model. The model is symmetric about the X-Z plane. Considering just one half of the model, 5 aerodynamic macro elements were used to describe the entire shape as presented in Figure 1. Plan and side views of the complete aerodynamic models are presented in Figure 2 and Figure 3. Figure 4 shows the location of the 101 structural grid points in comparison to the aerodynamic model. The connection between the front and rear fuselage section has not been modelled due to lack of data points in this section to estimate the dimensions accurately.

The aerodynamic forces were calculated over a range of reduced frequencies ranging from 0.02 to 1.5 at a series of Mach numbers. Infinite plate splines were used to transfer the aerodynamic forces to the structure. All non-collinear grid points supplied are used in the splining process, giving 99 usable points.

Currently two solution set-ups have been created: 1- Matched Flutter analysis and 2- Static analysis. Flutter analysis provides the frequency and damping throughout the flight enveloped. A matched solution is used by using the bulk data card FIXHATM. Trim analysis is set-up for a steady-state level flight condition at a specified angle of attack. Elastic and rigid deformations are obtained as well as lift and induced drag.

The Flutter analysis was performed at an altitude of 19812 metres (65000 ft) covering the Mach number range between 0.2 and 0.9. Typical frequency-damping plots are shown in Figure 5. Figure 6 highlights the damping plot near the flutter crossing. Flutter is estimated to occur at around 155 m/s.

Further modelling improvements can be obtained by: 1- Splining the mode shapes to obtain more grid points; 2- Camber effects can be introduced based on the supplied manufacturing drawings although these will not affect the panel method aerodynamics.

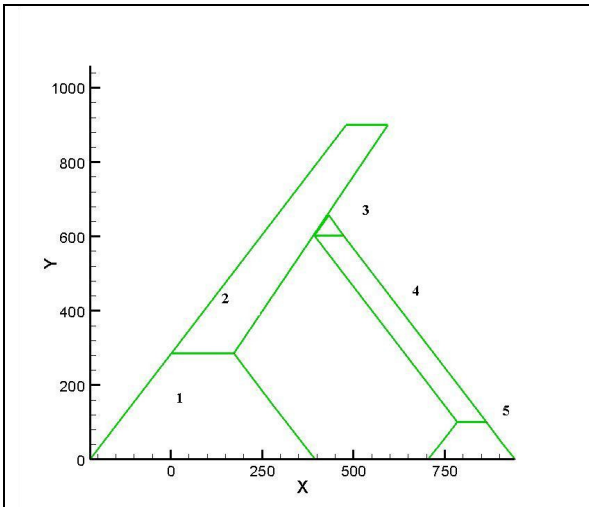

Figure 1 Macro-elements definition

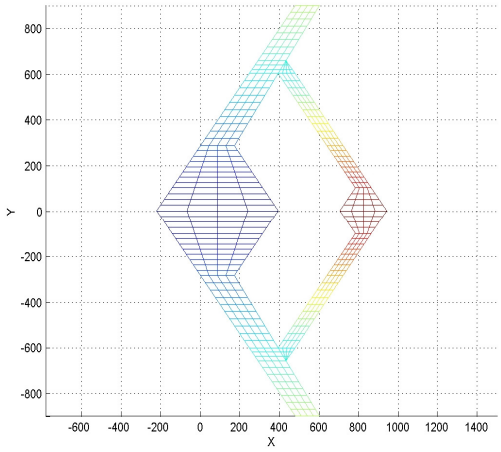

Figure 2 X-Y View

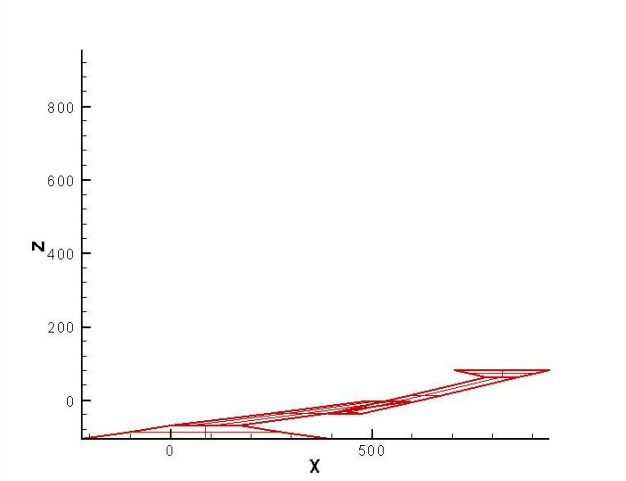

Figure 3 X-Z View

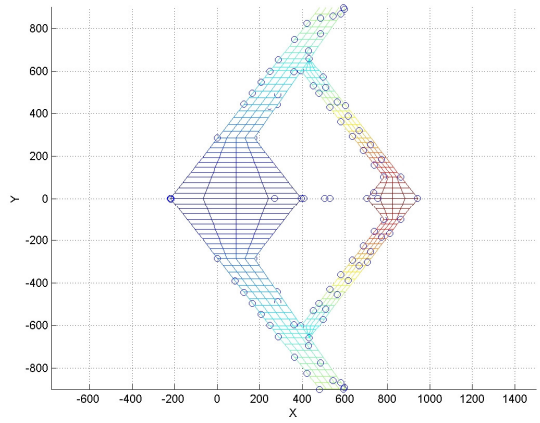

Figure 4 Aerodynamic mesh outline and FE grid points location

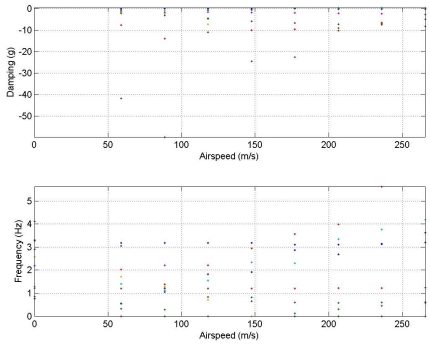

Figure 5 Frequency-Damping Plot at 19812 m

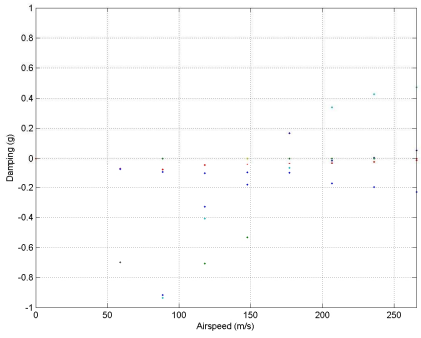

Figure 6 Damping plot at 19812 m - zoomed

3. AEROELASTIC SCALING APPROACH

In this chapter, the background to the aeroelastic scaling approach to be used for the design, manufacture and test of a sensorcraft aeroelastic model is described.

3.1 Objectives

To define a **dynamically** scaled aeroelastic model that responds identically to a full-scale design with respect to chosen scale factors (e.g. geometric scaling, velocity scaling etc). This goal can be achieved on the basis of a set of non-dimensional aeroelastic equations. A key requirement is to eliminate the reliance of the BAH scaling approach on equivalent beams as in this design case the scaled structure is topologically and materially different from the full-scale structure (we don't know anything about its internal structure).

3.2 Approach

Based on wind-tunnel parameters, identify the maximum geometry scale and maximum velocity scale. For a dynamically scaled test, will also need to identify a third scale (e.g. mass).

- Identify the governing non-dimensional equations of motion (EOM) that will be numerically identical for both the scaled and full-scale designs. The choice of degrees of freedom must serve both models. The common degrees of freedom may be reflected on a global scale with modal coordinates or a local scale with influence coefficients interpolated at common points.
- Start the scaled model design process by defining the flexible structure or the (to be) scaled model. This layout could be a lattice of beams (but not necessarily – could be ribs and spars, or perhaps an equivalent plate).
- Size the scaled model structure according to the scaling parameters. This step depends on the form of the governing aeroelastic equations of motion.

3.3 Non-Dimensionalised Aeroelastic Equations of Motion

In order to achieve a non-dimensional set of equations, we need to select 3 base units of measurement for dynamic analysis, typically mass, length and velocity (length / time) although force, length and velocity could also be chosen. For static analysis we only need 2 base units of measurement - force and length (the time dependent term is removed).

The following equations assume we have reduced the equations of motion to a minimum of two degrees of freedom that represent displacement (length) and rotation (non-dimensional). These two degrees of freedom are consistent with most commercial finite element codes.

Taking a coupled FE / Aerodynamic equations of motion (ignoring structural damping) such that

$$\begin{bmatrix} \mathbf{M}_{11} & \mathbf{M}_{12} \\ \mathbf{M}_{21} & \mathbf{M}_{22} \end{bmatrix} \begin{Bmatrix} \ddot{\mathbf{X}} \\ \ddot{\boldsymbol{\theta}} \end{Bmatrix} + \begin{bmatrix} \mathbf{K}_{11} & \mathbf{K}_{12} \\ \mathbf{K}_{21} & \mathbf{K}_{22} \end{bmatrix} \begin{Bmatrix} \mathbf{X} \\ \boldsymbol{\theta} \end{Bmatrix} = \frac{\rho \mathbf{V}^2}{2} \begin{bmatrix} \mathbf{b}^2 & 0 \\ 0 & \mathbf{b}^3 \end{bmatrix} \begin{bmatrix} \mathbf{Q}_{11} & \mathbf{Q}_{12} \\ \mathbf{Q}_{21} & \mathbf{Q}_{22} \end{bmatrix} \begin{Bmatrix} \mathbf{X} \\ \boldsymbol{\theta} \end{Bmatrix} \qquad (5)$$

where

$\mathbf{X}$	= Vector of translational degrees of freedom
$\boldsymbol{\theta}$	= Vector of rotational degrees of freedom
$\mathbf{M_{ij}}$	= Block matrix terms in inertia / mass matrix
$\mathbf{K_{ij}}$	= Block matrix terms in stiffness matrix
$\mathbf{b}$	= Reference length (semi-chord)
$\mathbf{Q_{ij}}$	= Block matrix Aerodynamic terms (complex for unsteady motions)

In terms of dimensions of the fundamental quantities (M, L, T) equation (5) has the form

$$\begin{bmatrix} \mathbf{M} & \mathbf{ML} \\ \mathbf{ML} & \mathbf{ML^2} \end{bmatrix} \begin{Bmatrix} \mathbf{LT^{-2}} \\ \mathbf{T^{-2}} \end{Bmatrix} + \begin{bmatrix} \mathbf{MT^{-2}} & \mathbf{MLT^{-2}} \\ \mathbf{MLT^{-2}} & \mathbf{ML^2T^{-2}} \end{bmatrix} \begin{Bmatrix} \mathbf{L} \\ \mathbf{ND} \end{Bmatrix} = \mathbf{ML^{-1}T^{-2}} \begin{bmatrix} \mathbf{L^2} & 0 \\ 0 & \mathbf{L^3} \end{bmatrix} \begin{bmatrix} \mathbf{L^{-1}} & \mathbf{ND} \\ \mathbf{L^{-1}} & \mathbf{ND} \end{bmatrix} \begin{Bmatrix} \mathbf{L} \\ \mathbf{ND} \end{Bmatrix} \tag{6}$$

Thus, according to Newtonian mechanics, we have three base scaling parameters of mass, length and time.

3.4 Base Scaling Parameters

Geometric Scaling: Defining the non-dimensional coordinate system (ξ, ϕ) such that

$$\mathbf{x = b\xi} \qquad \textbf{and} \qquad \boldsymbol{\theta = \phi} \tag{7}$$

Time Scaling: Using non-dimensional time $\tau = \dfrac{\mathbf{Vt}}{\mathbf{b}}$, the base time unit is indirectly scaled in terms of a (surrogate) velocity and geometric scale – which reflects the requirement that the scaled model operate within the wind tunnel operational limits. Use the chain rule to non-dimensionalize time derivatives that are present in the governing equations of motion.

$$\dot{\mathbf{x}} = \mathbf{V}\xi' \quad \ddot{\mathbf{x}} = \frac{\mathbf{V}^2}{\mathbf{b}}\xi'' \qquad \dot{\boldsymbol{\theta}} = \frac{\mathbf{V}}{\mathbf{b}}\phi' \qquad \ddot{\boldsymbol{\theta}} = \frac{\mathbf{V}^2}{\mathbf{b}^2}\phi'' \tag{8}$$

where (.) denotes differentiation w.r.t time and (‘) denotes differentiation w.r.t non-dimensional time.

Mass Scaling: There are a number of options for scaling the mass. These are discussed below. Mass can be scaled directly (e.g. total mass of the airplane). Mass can also be scaled in terms of a surrogate density scale. Also, since Force is mass times acceleration, units of force can be used as a derivative (or surrogate) scaling parameter for mass.

Equation (2) will be rendered non-dimensional according to the three scaling parameters.

3.5 Mass Scaling

The first approach will consider using some reference mass $\mathbf{m_r}$ as part of the scaling process.

Non-Dimensionalised Inertial Force

Defining non-dimensional inertia terms (denoted by the overbar)

$$\mathbf{M_{11} = m_r \bar{M}_{11} \qquad M_{12} = m_r b \bar{M}_{12} \qquad M_{21} = m_r b \bar{M}_{21} \qquad M_{22} = m_r b^2 \bar{M}_{22}} \tag{9}$$

where $\mathbf{m_r}$ is some reference mass (e.g. total mass of the full structure) then the force and moment resulting from the mass and inertial terms can be written as

$$\begin{Bmatrix} \mathbf{F} \\ \mathbf{M} \end{Bmatrix}_{\mathbf{I}} = \begin{pmatrix} \mathbf{M_{11}} & \mathbf{M_{12}} \\ \mathbf{M_{21}} & \mathbf{M_{22}} \end{pmatrix} \begin{Bmatrix} \ddot{\mathbf{x}} \\ \ddot{\boldsymbol{\theta}} \end{Bmatrix} = \begin{pmatrix} \mathbf{m_r \bar{M}_{11}} & \mathbf{m_r b \bar{M}_{12}} \\ \mathbf{m_r b \bar{M}_{21}} & \mathbf{m_r b^2 \bar{M}_{22}} \end{pmatrix} \begin{Bmatrix} \dfrac{\mathbf{V}^2}{\mathbf{b}} \boldsymbol{\xi}'' \\ \dfrac{\mathbf{V}^2}{\mathbf{b}^2} \boldsymbol{\phi}'' \end{Bmatrix} \tag{10}$$

thus

$$\begin{aligned} \begin{Bmatrix} \mathbf{F} \\ \mathbf{M} \end{Bmatrix}_{\mathbf{I}} &= \begin{pmatrix} \dfrac{\mathbf{m_r V^2}}{\mathbf{b}} \bar{\mathbf{M}}_{11} & \dfrac{\mathbf{m_r V^2}}{\mathbf{b}} \bar{\mathbf{M}}_{12} \\ \mathbf{m_r V^2 \bar{M}_{21}} & \mathbf{m_r V^2 \bar{M}_{22}} \end{pmatrix} \begin{Bmatrix} \boldsymbol{\xi}'' \\ \boldsymbol{\phi}'' \end{Bmatrix} = \begin{pmatrix} \dfrac{\mathbf{m_r V^2}}{\mathbf{b}} & 0 \\ 0 & \mathbf{m_r V^2} \end{pmatrix} \begin{pmatrix} \bar{\mathbf{M}}_{11} & \bar{\mathbf{M}}_{12} \\ \bar{\mathbf{M}}_{21} & \bar{\mathbf{M}}_{22} \end{pmatrix} \begin{Bmatrix} \boldsymbol{\xi}'' \\ \boldsymbol{\phi}'' \end{Bmatrix} \\ &= \begin{pmatrix} \dfrac{\mathbf{m_r V^2}}{\mathbf{b}} & 0 \\ 0 & \mathbf{m_r V^2} \end{pmatrix} \begin{Bmatrix} \bar{\mathbf{F}} \\ \bar{\mathbf{M}} \end{Bmatrix}_{\mathbf{I}} \end{aligned} \tag{11}$$

where $\bar{\mathbf{F}}$ and $\bar{\mathbf{M}}$ are non-dimensional forces and moments respectively.

Non-Dimensionalised Stiffness Force

The process for the stiffness terms follows the same procedure as that shown above for the inertia terms, still making use of the same reference mass as before. Defining

$$\mathbf{K_{11} = \frac{m_r V^2}{b^2} \bar{K}_{11} \qquad K_{12} = \frac{m_r V^2}{b} \bar{K}_{12} \qquad K_{21} = \frac{m_r V^2}{b} \bar{K}_{21} \qquad K_{22} = m_r V^2 \bar{K}_{22}} \tag{12}$$

then the force and moment resulting from the stiffness terms can be written as

$$\begin{Bmatrix} \mathbf{F} \\ \mathbf{M} \end{Bmatrix}_{\mathbf{S}} = \begin{pmatrix} \mathbf{K_{11}} & \mathbf{K_{12}} \\ \mathbf{K_{21}} & \mathbf{K_{22}} \end{pmatrix} \begin{Bmatrix} \mathbf{x} \\ \boldsymbol{\theta} \end{Bmatrix} = \begin{pmatrix} \dfrac{\mathbf{m_r V^2}}{\mathbf{b}^2} \bar{\mathbf{K}}_{11} & \dfrac{\mathbf{m_r V^2}}{\mathbf{b}} \bar{\mathbf{K}}_{12} \\ \dfrac{\mathbf{m_r V^2}}{\mathbf{b}} \bar{\mathbf{K}}_{21} & \mathbf{m_r V^2 \bar{K}_{22}} \end{pmatrix} \begin{Bmatrix} \mathbf{b}\boldsymbol{\xi} \\ \boldsymbol{\phi} \end{Bmatrix} \tag{13}$$

thus

$$\begin{Bmatrix} \mathbf{F} \\ \mathbf{M} \end{Bmatrix}_s = \begin{pmatrix} \frac{\mathbf{m_r V^2}}{\mathbf{b}} \bar{\mathbf{K}}_{11} & \frac{\mathbf{m_r V^2}}{\mathbf{b}} \bar{\mathbf{K}}_{12} \\ \mathbf{m_r V^2} \bar{\mathbf{K}}_{21} & \mathbf{m_r V^2} \bar{\mathbf{K}}_{22} \end{pmatrix} \begin{Bmatrix} \xi \\ \phi \end{Bmatrix} = \begin{pmatrix} \frac{\mathbf{m_r V^2}}{\mathbf{b}} & 0 \\ 0 & \mathbf{m_r V^2} \end{pmatrix} \begin{pmatrix} \bar{\mathbf{K}}_{11} & \bar{\mathbf{K}}_{12} \\ \bar{\mathbf{K}}_{21} & \bar{\mathbf{K}}_{22} \end{pmatrix} \begin{Bmatrix} \xi \\ \phi \end{Bmatrix}$$
$$= \begin{pmatrix} \frac{\mathbf{m_r V^2}}{\mathbf{b}} & 0 \\ 0 & \mathbf{m_r V^2} \end{pmatrix} \begin{Bmatrix} \bar{\mathbf{F}} \\ \bar{\mathbf{M}} \end{Bmatrix}_s \tag{14}$$

Non-Dimensionalised Aeroelastic Equations

Introducing transformations (7) and (8) into equation (5) and pre-multiplying by

$$\Psi = \begin{pmatrix} \frac{\mathbf{b}}{\mathbf{m_r V^2}} & 0 \\ 0 & \frac{1}{\mathbf{m_r V^2}} \end{pmatrix} \tag{15}$$

gives the redefined system equations as

$$\begin{bmatrix} \bar{\mathbf{M}}_{11} & \bar{\mathbf{M}}_{12} \\ \bar{\mathbf{M}}_{21} & \bar{\mathbf{M}}_{22} \end{bmatrix} \begin{Bmatrix} \xi'' \\ \phi'' \end{Bmatrix} + \begin{bmatrix} \bar{\mathbf{K}}_{11} & \bar{\mathbf{K}}_{12} \\ \bar{\mathbf{K}}_{21} & \bar{\mathbf{K}}_{22} \end{bmatrix} \begin{Bmatrix} \xi \\ \phi \end{Bmatrix} = \begin{bmatrix} \frac{\rho \mathbf{b}^3}{2\mathbf{m_r}} & 0 \\ 0 & \frac{\rho \mathbf{b}^3}{2\mathbf{m_r}} \end{bmatrix} \begin{bmatrix} \mathbf{bQ}_{11} & \mathbf{Q}_{12} \\ \mathbf{bQ}_{21} & \mathbf{Q}_{22} \end{bmatrix} \begin{Bmatrix} \xi \\ \phi \end{Bmatrix} \tag{16}$$

Note that the Q matrix now becomes fully non-dimensional.

3.6 Density Scaling

A second approach will consider using the air density as part of the scaling process

Non-Dimensionalised Inertial Force

Defining non-dimensional inertia terms (denoted by the overbar)

$$\mathbf{M}_{11} = \rho \mathbf{b}^3 \bar{\mathbf{M}}_{11} \qquad \mathbf{M}_{12} = \rho \mathbf{b}^4 \bar{\mathbf{M}}_{12} \qquad \mathbf{M}_{21} = \rho \mathbf{b}^4 \bar{\mathbf{M}}_{21} \qquad \mathbf{M}_{22} = \rho \mathbf{b}^5 \bar{\mathbf{M}}_{22} \tag{17}$$

where ρ is the air density and $\mathbf{b}$ is some defined length, then the force and moment resulting from the mass and inertial terms can be written as

$$\begin{Bmatrix} \mathbf{F} \\ \mathbf{M} \end{Bmatrix}_I = \begin{pmatrix} \mathbf{M}_{11} & \mathbf{M}_{12} \\ \mathbf{M}_{21} & \mathbf{M}_{22} \end{pmatrix} \begin{Bmatrix} \ddot{\mathbf{x}} \\ \ddot{\theta} \end{Bmatrix} = \begin{pmatrix} \rho \mathbf{b}^3 \bar{\mathbf{M}}_{11} & \rho \mathbf{b}^4 \bar{\mathbf{M}}_{12} \\ \rho \mathbf{b}^4 \bar{\mathbf{M}}_{21} & \rho \mathbf{b}^5 \bar{\mathbf{M}}_{22} \end{pmatrix} \begin{Bmatrix} \frac{\mathbf{V}^2}{\mathbf{b}} \xi'' \\ \frac{\mathbf{V}^2}{\mathbf{b}^2} \phi'' \end{Bmatrix} \tag{18}$$

thus

$$\begin{Bmatrix} \mathbf{F} \\ \mathbf{M} \end{Bmatrix}_{\mathbf{I}} = \begin{pmatrix} \rho V^2 b^2 \bar{M}_{11} & \rho V^2 b^2 \bar{M}_{12} \\ \rho V^2 b^3 \bar{M}_{21} & \rho V^2 b^3 \bar{M}_{22} \end{pmatrix} \begin{Bmatrix} \xi'' \\ \phi'' \end{Bmatrix} = \begin{pmatrix} \rho V^2 b^2 & 0 \\ 0 & \rho V^2 b^3 \end{pmatrix} \begin{pmatrix} \bar{M}_{11} & \bar{M}_{12} \\ \bar{M}_{21} & \bar{M}_{22} \end{pmatrix} \begin{Bmatrix} \xi'' \\ \phi'' \end{Bmatrix}$$
$$= \begin{pmatrix} \rho V^2 b^2 & 0 \\ 0 & \rho V^2 b^3 \end{pmatrix} \begin{Bmatrix} \bar{F} \\ \bar{M} \end{Bmatrix}_{\mathbf{I}} \tag{19}$$

where $\bar{F}$ and $\bar{M}$ are non-dimensional forces and moments respectively.

Non-Dimensionalised Stiffness Force

The process for the stiffness terms follows the same procedure as that shown above for the inertia terms. Defining

$$K_{11} = \rho b V^2 \bar{K}_{11} \qquad K_{12} = \rho b^2 V^2 \bar{K}_{12} \qquad K_{21} = \rho b^2 V^2 \bar{K}_{21} \qquad K_{22} = \rho b^3 V^2 \bar{K}_{22} \tag{20}$$

then the force and moment resulting from the stiffness terms can be written as

$$\begin{Bmatrix} \mathbf{F} \\ \mathbf{M} \end{Bmatrix}_{\mathbf{S}} = \begin{pmatrix} K_{11} & K_{12} \\ K_{21} & K_{22} \end{pmatrix} \begin{Bmatrix} x \\ \theta \end{Bmatrix} = \begin{pmatrix} \rho b V^2 \bar{K}_{11} & \rho b^2 V^2 \bar{K}_{12} \\ \rho b^2 V^2 \bar{K}_{21} & \rho b^3 V^2 \bar{K}_{22} \end{pmatrix} \begin{Bmatrix} b\xi \\ \phi \end{Bmatrix} \tag{21}$$

thus

$$\begin{Bmatrix} \mathbf{F} \\ \mathbf{M} \end{Bmatrix}_{\mathbf{S}} = \begin{pmatrix} \rho b^2 V^2 \bar{K}_{11} & \rho b^2 V^2 \bar{K}_{12} \\ \rho b^3 V^2 \bar{K}_{21} & \rho b^3 V^2 \bar{K}_{22} \end{pmatrix} \begin{Bmatrix} \xi \\ \phi \end{Bmatrix} = \begin{pmatrix} \rho b^2 V^2 & 0 \\ 0 & \rho b^3 V^2 \end{pmatrix} \begin{pmatrix} \bar{K}_{11} & \bar{K}_{12} \\ \bar{K}_{21} & \bar{K}_{22} \end{pmatrix} \begin{Bmatrix} \xi \\ \phi \end{Bmatrix}$$
$$= \begin{pmatrix} \rho b^2 V^2 & 0 \\ 0 & \rho b^3 V^2 \end{pmatrix} \begin{Bmatrix} \bar{F} \\ \bar{M} \end{Bmatrix}_{\mathbf{S}} \tag{22}$$

Non-Dimensionalised Aeroelastic Equations

Introducing transformations (17) and (20) and pre-multiplying equation (5) by

$$\Psi = \begin{pmatrix} \dfrac{1}{\rho b^2 V^2} & 0 \\ 0 & \dfrac{1}{\rho b^3 V^2} \end{pmatrix} \tag{23}$$

gives the redefined system equations as

$$\begin{bmatrix} \bar{M}_{11} & \bar{M}_{12} \\ \bar{M}_{21} & \bar{M}_{22} \end{bmatrix} \begin{Bmatrix} \xi'' \\ \phi'' \end{Bmatrix} + \begin{bmatrix} \bar{K}_{11} & \bar{K}_{12} \\ \bar{K}_{21} & \bar{K}_{22} \end{bmatrix} \begin{Bmatrix} \xi \\ \phi \end{Bmatrix} = \begin{bmatrix} 1/2 & 0 \\ 0 & 1/2 \end{bmatrix} \begin{bmatrix} bQ_{11} & Q_{12} \\ bQ_{21} & Q_{22} \end{bmatrix} \begin{Bmatrix} \xi \\ \phi \end{Bmatrix} \tag{24}$$

Again, the Q matrix now becomes fully non-dimensional. It is arguable that this is a better form to use as there is only a length scaling that needs to be changed, however, there are now no longer any density or mass terms directly visible in equation (24).

3.7 Use of Modal Transformation

It is usual to make use of a modal transformation to reduce the size of the equations (matrix dimensions m x m, where m = number of physical degrees of freedom) that are being dealt with, otherwise system equations (16) and (24) can be very large. Consider equation (24), then making use of the non-dimensional transformation

$$\begin{Bmatrix} \boldsymbol{\xi} \\ \boldsymbol{\phi} \end{Bmatrix} = \boldsymbol{\Psi} \begin{Bmatrix} \hat{\boldsymbol{\xi}} \\ \hat{\boldsymbol{\phi}} \end{Bmatrix} \tag{25}$$

where $\boldsymbol{\Psi}$ are the first n eigenvectors (columns) of (non-dimensional) matrix

$$\left\{ \begin{bmatrix} \bar{\mathbf{M}}_{11} & \bar{\mathbf{M}}_{12} \\ \bar{\mathbf{M}}_{21} & \bar{\mathbf{M}}_{22} \end{bmatrix}^{-1} \begin{bmatrix} \bar{\mathbf{K}}_{11} & \bar{\mathbf{K}}_{12} \\ \bar{\mathbf{K}}_{21} & \bar{\mathbf{K}}_{22} \end{bmatrix} \right\} \tag{26}$$

and usually n (modes that are considered) << m, then the non-dimensional modal system equations become

$$\begin{bmatrix} \hat{\mathbf{M}}_{11} & 0 \\ 0 & \hat{\mathbf{M}}_{22} \end{bmatrix} \begin{Bmatrix} \hat{\boldsymbol{\xi}}'' \\ \hat{\boldsymbol{\phi}}'' \end{Bmatrix} + \begin{bmatrix} \hat{\mathbf{K}}_{11} & 0 \\ 0 & \hat{\mathbf{K}}_{22} \end{bmatrix} \begin{Bmatrix} \hat{\boldsymbol{\xi}} \\ \hat{\boldsymbol{\phi}} \end{Bmatrix} = \boldsymbol{\Psi}^{\mathrm{T}} \begin{bmatrix} 1/2 & 0 \\ 0 & 1/2 \end{bmatrix} \begin{bmatrix} \mathbf{bQ}_{11} & \mathbf{Q}_{12} \\ \mathbf{bQ}_{21} & \mathbf{Q}_{22} \end{bmatrix} \boldsymbol{\Psi} \begin{Bmatrix} \hat{\boldsymbol{\xi}} \\ \hat{\boldsymbol{\phi}} \end{Bmatrix} \tag{27}$$

with a similar result being found if system equations (16) were considered. Inertia and stiffness terms $\hat{\mathbf{M}}, \hat{\mathbf{K}}$ are diagonal matrices. The non-dimensional modal coordinates $\hat{\boldsymbol{\xi}}, \hat{\boldsymbol{\phi}}$ do not relate directly to a particular physical coordinate but only via the linear transformation in equation (25). As the modal transformation has been applied to non-dimensional equations, then the modal equations are also non-dimensional and can therefore be used directly in the scaling process.

3.8 Scaling of the Aeroelastic Equations

We have arrived at two different non-dimensional sets of aeroelastic equations (16) and (24). These equations can be used to determine the system behaviour for any combination of fundamental quantities $\boldsymbol{\rho}, \mathbf{b}, \mathbf{m}_r$ or $\boldsymbol{\rho}, \mathbf{b}, \mathbf{V}$ respectively using the scaling relationships (9) and (12) or (17) and (20) respectively. If the full size and model structure (physical construction and FE / aerodynamic models) are exactly the same, then these scaling relationships determine the scaled model characteristics. The following comments also apply directly to aeroelastic system equations in modal coordinates.

However, in practice the model structure is not constructed in the same way as the full size aircraft, and the finite element and aerodynamic models will also not be the same therefore the above scaling relationships can be used to provide "target" characteristics for the scaled model. For the rest of this section the mass scaling approach will be used but the density scaling approach, or any other, could be used as well.

Wind-Off Natural Frequencies and Mode Shapes

The natural frequencies and corresponding mode shapes of the full scale system are obtained from the eigensolution of the matrix

$$\mathbf{D}\boldsymbol{\Phi} = \boldsymbol{\Phi}\boldsymbol{\Omega} \tag{28}$$

where

$$\mathbf{D} = \begin{bmatrix} \mathbf{M}_{11} & \mathbf{M}_{12} \\ \mathbf{M}_{21} & \mathbf{M}_{22} \end{bmatrix}^{-1} \begin{bmatrix} \mathbf{K}_{11} & \mathbf{K}_{12} \\ \mathbf{K}_{21} & \mathbf{K}_{22} \end{bmatrix}$$

$$\boldsymbol{\Omega} = \mathbf{diag}\left[\omega_1^2, \omega_2^2, \ \ldots \omega_N^2\right] \ \ (\mathbf{eigenvalues}) \tag{29}$$

$$\boldsymbol{\Phi} = \left[\{\phi_1\}, \{\phi_2\}, \ \ldots \{\phi_N\}\right] \ \ (\mathbf{eigenvectors = mode\ shapes})$$

and the natural frequencies have units of rad s^{-1} whereas the mode shapes are non-dimensional.

In terms of the non-dimensionalised equations of motion (taking the mass scaling route), the natural frequencies and corresponding mode shapes are obtained from the eigensolution of the matrix

$$\bar{\mathbf{D}}\bar{\boldsymbol{\Phi}} = \bar{\boldsymbol{\Phi}}\bar{\boldsymbol{\Omega}} \tag{30}$$

where

$$\bar{\mathbf{D}} = \begin{bmatrix} \bar{\mathbf{M}}_{11} & \bar{\mathbf{M}}_{12} \\ \bar{\mathbf{M}}_{21} & \bar{\mathbf{M}}_{22} \end{bmatrix}^{-1} \begin{bmatrix} \bar{\mathbf{K}}_{11} & \bar{\mathbf{K}}_{12} \\ \bar{\mathbf{K}}_{21} & \bar{\mathbf{K}}_{22} \end{bmatrix}$$

$$\bar{\boldsymbol{\Omega}} = \mathbf{diag}\left[\bar{\omega}_1^2, \bar{\omega}_2^2, \ \ldots \bar{\omega}_N^2\right] \ \ (\mathbf{eigenvalues}) \tag{31}$$

$$\bar{\boldsymbol{\Phi}} = \left[\{\phi_1\}, \{\phi_2\}, \ \ldots \{\phi_N\}\right] = \boldsymbol{\Phi} \ \ (\mathbf{eigenvectors = mode\ shapes})$$

and the natural frequencies now have units of rad τ^{-1}. Unfortunately at zero airspeed the scaling has no meaning and therefore the dynamic analysis must be performed with the inclusion of the velocity dependent aerodynamic terms.

Wind-on Natural Frequencies and Mode Shapes

Considering the system when there is some airspeed, the non-dimensionalised frequencies, dampings and mode shapes are found from the solution of

$$\begin{bmatrix} \bar{\mathbf{M}}_{11} & \bar{\mathbf{M}}_{12} \\ \bar{\mathbf{M}}_{21} & \bar{\mathbf{M}}_{22} \end{bmatrix} \begin{Bmatrix} \xi'' \\ \phi'' \end{Bmatrix} + \left(\begin{bmatrix} \bar{\mathbf{K}}_{11} & \bar{\mathbf{K}}_{12} \\ \bar{\mathbf{K}}_{21} & \bar{\mathbf{K}}_{22} \end{bmatrix} - \begin{bmatrix} \dfrac{\rho b^3}{2m_r} & 0 \\ 0 & \dfrac{\rho b^3}{2m_r} \end{bmatrix} \begin{bmatrix} \mathbf{bQ}_{11} & \mathbf{Q}_{12} \\ \mathbf{bQ}_{21} & \mathbf{Q}_{22} \end{bmatrix} \right) \begin{Bmatrix} \xi \\ \phi \end{Bmatrix} = \begin{Bmatrix} 0 \\ 0 \end{Bmatrix} \tag{32}$$

Although the structural terms remain the same whatever the scaling, the aerodynamic terms do change depending upon the triple (m_r, ρ, b). Remember that the frequencies that are obtained are in non-dimensional time and thus are scaled by $\mathbf{b}/\mathbf{V}$ (i.e. the term $\dfrac{\boldsymbol{\omega}\mathbf{b}}{\mathbf{V}}$ remains constant) and that the mode shapes (a set of non-dimensional ratios) are complex.

Static Aeroelastic Deflections

The static aeroelastic deflections depend upon there being some initial incidence on some parts of the lifting surfaces. In terms of the non-dimensionalised equations (32) we get

$$\left(\begin{bmatrix} \bar{\mathbf{K}}_{11} & \bar{\mathbf{K}}_{12} \\ \bar{\mathbf{K}}_{21} & \bar{\mathbf{K}}_{22} \end{bmatrix} - \begin{bmatrix} \frac{\rho b^3}{2m_r} & 0 \\ 0 & \frac{\rho b^3}{2m_r} \end{bmatrix} \begin{bmatrix} bQ_{11} & Q_{12} \\ bQ_{21} & Q_{22} \end{bmatrix} \right) \begin{Bmatrix} \xi \\ \phi \end{Bmatrix} = \begin{bmatrix} \frac{\rho b^3}{2m_r} & 0 \\ 0 & \frac{\rho b^3}{2m_r} \end{bmatrix} \begin{bmatrix} bQ_{11} & Q_{12} \\ bQ_{21} & Q_{22} \end{bmatrix} \begin{Bmatrix} 0 \\ \phi_0 \end{Bmatrix} \quad (33)$$

where ϕ_0 are a set of initial angles of incidence. The deflections ξ, ϕ that are found are still non-dimensional.

4. Practical Application of Aeroelastic Scaling

In practice, the problem is defined as to find an equivalent aeroelastically scaled model structure given the FE and aerodynamic models of a full scale structure at specified flight conditions. Although the geometric scaling holds for the planform of the model, the internal structure is likely to be different, possibly not even made of the same material or construction technique; similarly, the FE and aerodynamic models corresponding to the scaled structure will also be different. The wind tunnel chosen to perform the tests will constrain the dimensions of the model and the speed it is tested at.

The differences between the full scale (subscript s) and model (subscript m - physical and computational) mean that it is not possible to simply scale the FE matrices. Instead comparison must be made of quantities such as modal parameters (frequencies and mode shapes), influence coefficients and non-dimensionalised deflections.

Here it is proposed to use the following scaled quantities.

4.1 Test Scaling Parameters

There are three scaling values that are defined by the difference in the required design configuration (i.e. wind tunnel parameters) and the original flight condition. Note that the differences in the Reynolds number will be ignored and it is assumed that the flow conditions between the full-size and scaled conditions have no effect upon the aeroelastic parameters.

Geometric Scaling

$$\mathbf{L_s = n_g L_m} \quad (34)$$

Velocity Scaling

$$\mathbf{V_s = n_v V_m} \quad (35)$$

Air Density Scaling

$$\boldsymbol{\rho_s = n_\rho \rho_m} \quad (36)$$

Typically n_g, $n_v > 1$ whereas $n_\rho < 1$. Note that the Equivalent Air Speed could be used in order to eliminate the need for density information.

Other Scaling Parameters

In order to achieve aeroelastic scaling, there is a need to scale in terms of the stiffness and the mass distributions. For an aircraft model that is simply "shrunk", or has an internal structure that is exactly the same as the full aircraft (as per BAH approach) then this is not a difficult process. In the case that

we are considering whereby the internal structure of the scaled model differs from the full size model, at least two of the following parameters must be chosen as part of the scaling process.

Reduced Frequencies

Rewriting the aeroelastic equations in non-dimensional form involves the transformation into non-dimensional time. The natural frequencies of the full-scale and model structure at the reference test conditions must be the same, thus

$$\frac{\omega_s b_s}{V_s} = \frac{\omega_m b_m}{V_m} \quad \Rightarrow \quad \omega_m = \frac{V_m}{V_s}\frac{b_s}{b_m}\omega_s = \frac{n_s}{n_v}\omega_s \tag{37}$$

i.e. the reduced frequencies must remain the same. The reduced frequencies depend upon a correct mass and stiffness distribution.

Mode Shapes

The mode shapes corresponding to the various natural frequencies of the full scale and model structure must be the same. These shapes will be complex to some degree depending upon the characteristics of the unsteady aerodynamics terms. As with the reduced frequencies, the mode shapes will depend upon obtaining a correct mass and stiffness distribution. It would be possible to compare the wind-off mode shapes for the full-size and scaled models which would eliminate any difficulties associated with more shape complexity.

Flutter Speed

The reduced frequency will remain the same for the full-size and scaled models, even at the flutter speed. Consequently it is possible to make a comparison of what the flutter speed should be based upon the velocity scaling rule. However, caution should be made when simply comparing the flutter speed as this does not infer that the entire aeroelastic characteristics have been captured.

Static Aeroelastic Deflections

The non-dimensionalised static aeroelastic equations (33) show that equivalent non-dimensionalised deflections at the reference test conditions must be the same. e.g. for the wing tip at the reference conditions

$$\left(\frac{x_{tip}}{b}\right)_s = \left(\frac{x_{tip}}{b}\right)_m \tag{38}$$

The static aeroelastic deflections will depend upon getting the stiffness distribution correctly. One advantage of comparing the static deflections wind-on is that there an implied scaling of the aerodynamic forces which would not occur for the wind-off case.

Flexibility Influence Coefficients

One method to get around the problem of determining the correct scaling of the aerodynamic loads is to determine the flexibility influence coefficients for the wind-off case at certain reference points on the structure (as per Mark French PhD [12]). This will give the correct stiffness distribution however, it does not take into account the changes in the aerodynamic forces.

Mass Scaling

The traditional approach for mass scaling is to non-dimensionalise the relationship between some reference mass (e.g. total mass) of the aircraft with that of the air. Typically this can be written as

$$\left(\frac{\mathbf{M}}{\rho \mathbf{b}^3}\right)_{\mathbf{s}} = \left(\frac{\mathbf{M}}{\rho \mathbf{b}^3}\right)_{\mathbf{m}} \quad \Rightarrow \quad \mathbf{M_m} = \frac{\mathbf{M_s}}{\mathbf{n_\rho n_g^3}} \tag{39}$$

Although this approach is fine for determining the overall mass, there are concerns when this is applied to a scaled model when the internal structure differs from the full-scale. Although the mass scaling gives a *necessary* condition for the scaling, there is no reference to the mass distribution (unless implied by having the same internal structure) and consequently it is not a *sufficient* condition for perfect mass scaling. Note how this term appears in the mass scaling approach described above to give equation (16).

4.2 Other Scaling Parameters of Interest

The above schemes are all related to a linear model and relate to what may be thought of as a conventional aeroelastic scaling approach. It is possible that several other parameters may have to be considered.

Gust Response

Gust velocities will scale in the same way as the airspeed. In order to achieve an equivalent scaled response, the same maximum normalised deflection to the scaled gust (e.q. "1 – cosine") at certain reference points of the structure must be obtained.

$$\left(V_{gust}\right)_s = n_v \left(V_{gust}\right)_m \qquad \left(\frac{x\,max_{tip}}{b}\right)_s = \left(\frac{x\,max_{tip}}{b}\right)_m \tag{40}$$

Non-Linear Static Aeroelastic Deflections

Although the FE model of a non-linear analysis (e.g. the non-linear geometric deflections that occur on a sensorcraft) is much more complicated than the linear description shown above, a similar scaling approach can be used. In the same way as for the linear static aeroelastic deflections, the equivalent non-dimensionalised non-linear deflections at the reference test conditions must be the same. e.g. for the wing tip at the reference conditions

$$\left(\frac{x_{tip}}{b}\right)_s = \left(\frac{x_{tip}}{b}\right)_m \tag{41}$$

and this will enable any non-linear deflection behaviour to be scaled.

Buckling

The critical speed at which buckling (linear or non-linear) will occur simply depends upon the velocity scaling

$$\left(V_{buckling}\right)_s = n_v \left(V_{buckling}\right)_m \tag{42}$$

and the critical buckling shape must be the same in a similar way to the mode shapes.

5. Optimisation Approach

An initial baseline scaled model was set up with the correct geometrically scaled planform and flight condition. The model was of such a design to enable efficient manufacture i.e. a simple 2 spar per wing design with uniform non-tapered wing section. (Such an approach was seen as a vast improvement upon the structure that was built and tested statically (see later) that was designed purely with the aeroelastic scaling as the dominant design driver, with no consideration of the manufacturing aspects.) The aeroelastically scaled model can then be found by determining what sizing of internal structure (spars and ribs), skin thickness and (possibly) extra distributed masses is required in order to achieve some set of defined non-dimensionalised functions. A Genetic Algorithm based approach was used, however, other evolutionary or hill-climbing optimisation algorithms could be used.

There are a large number of possible target functions that can be chosen from the list above and, as the internal structure will not be a shrunk version of the full-scale sensorcraft, it is unlikely that an exact match will be obtained for all conditions. For this initial design study, only the minimum number of parameters (one mass and one stiffness condition) required at a single test condition and few modes were considered. The scaled model was aimed to be tested at 30 m/s, a condition that could easily be achieved in the '9x7' wind tunnel at the Goldstein Wind Tunnel Laboratory of the University of Manchester where it was intended to test the model.

5.1 Baseline Finite Element Sensorcraft Model

A baseline finite element model of a Sensorcraft type aircraft was developed for use in the aeroelastic scaling process and eventual manufacture and test of a Sensorcraft wind tunnel model. The Finite Element model was developed in a manner that will be consistent with an efficient manufacturing process and consists of two spars along each wing, whose dimensions can be varied along the span, attached with ribs whose thickness can be altered as part of the scaling process. It was constructed in order to size the wind tunnel model dimensions for spar, ribs and skin thickness.

5.2 Geometric Scaling

The scaled model will be a factor of 12 smaller than the full scale model (semi-span = 18.285m, length = 23.64m) and so the semi-span of the scaled (half) model becomes 1.5237 metres and the overall length is 1.97 metres.

5.3 Finite Element Model

A MATLAB code was created in order to define the "deck" used to build the NASTRAN FE model.
The model consists of the following elements:

- Skin modelled using shell elements. The airfoil shape is currently based on the NACA0012 shape, but this can be changed to any other profile.
- Two plates, modelled as quadrilateral elements, are included to model the front and rear fuselage sections.
- Beam elements are used to model the spars and are located at 25% and 75% chord along the span of the model on both front and rear wing sections.
- The junction area between the two wings is modelled by creating an airfoil decreasing in chord length. It was assumed that the beams would pass through the rib at the joining between the respective rib and the spars in the front fuselage. This is the most difficult part of the manufacturing process and may require a further change in the future once detailed consideration of the manufacturing of the joined wing is considered.
- The connection between front and rear fuselage section is modelled using beam elements.

- The model is fully clamped at the front fuselage section, while the rear fuselage section is free to move in the Z direction and rotate around the X and Y axes.
- The material properties assigned to all the elements is aluminium alloy.

There are a number of variable parameters to approximate the FE model, i.e. the number of nodes describing the airfoil, the number of beam elements between each rib. Also the number of elements describing the fuselage sections and the number of quadrilateral elements describing the skin between each rib are all variable. Initial convergence studies have enabled the correct element density to be determined. The external skin mesh is shown in figure 6 and figures 7-9 show various views of the internal structure.

Each rib has its own properties (thickness) that can be assigned via the deck. The fuselage plates, skin of the front wing, the skin of the rear and the beams have different (geometric) properties that can also be assigned. It is assumed that the shell elements have a uniform thickness throughout each of the elements. The beams that make up the spars and also the connection between the front and real fuselage are assumed to be rectangular, so that height and width only need to be defined between each rib. Manufacturing and computational considerations are likely to mean that the structure is divided into different regions that have the same geometric properties rather than changing the properties of every element.

An initial calculation was performed to determine whether the dynamic behaviour looked sensible; the following properties were assigned to the various elements:

- spars height 0.1m
- spars width 0.03m
- rib thickness 0.03m
- skin thickness 0.001m
- Fuselage section plate thickness 0.1m

and the first four mode shapes are displayed in figures 10-13. The mode shapes are more or less what would be expected although, of course, the structural parameters will need to be changed in order to achieve the aeroelastically scaled model, as described above. Again, it must be stressed that these calculations have been performed to get an idea of how the model behaves and are <u>not</u> at this stage scaled estimates.

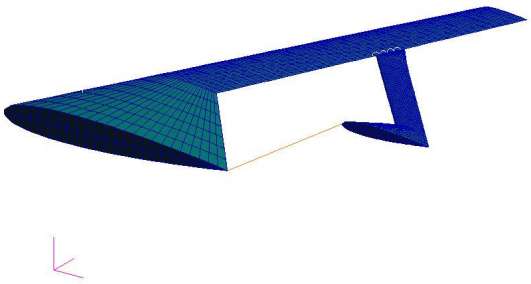

Figure 6 XYZ View Full FE model external surface

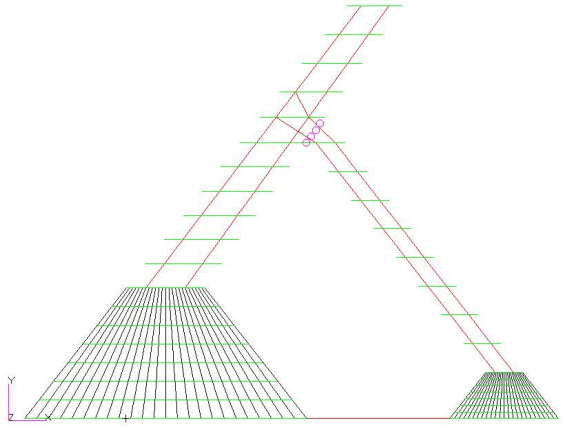

Figure 7 XY View internal structure FE model

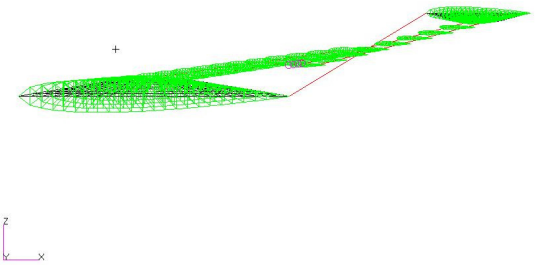

Figure 8 XZ View internal structure FE model

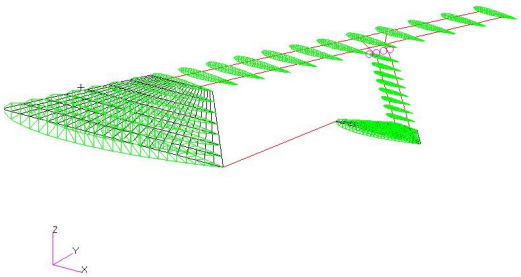

Figure 9 XYZ View internal structure of FE model

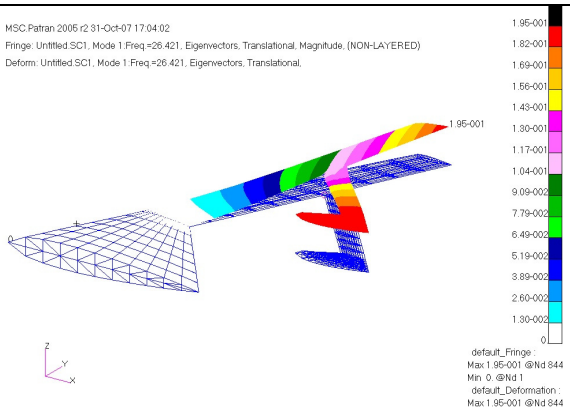

Figure 10 Scaled Sensorcraft model Mode 1 26.4 Hz

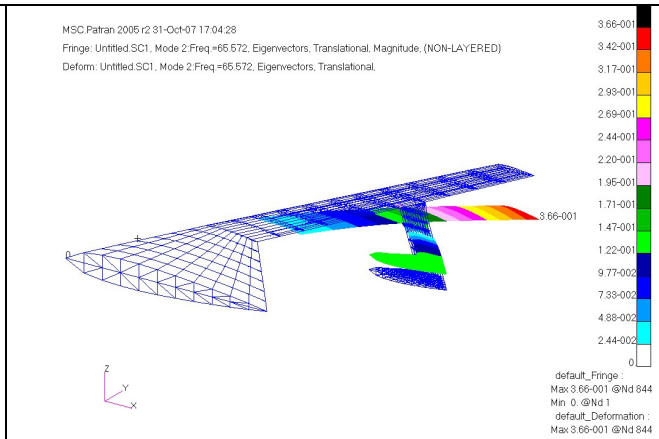

Figure 11 Scaled Sensorcraft model Mode 2 65.5 Hz

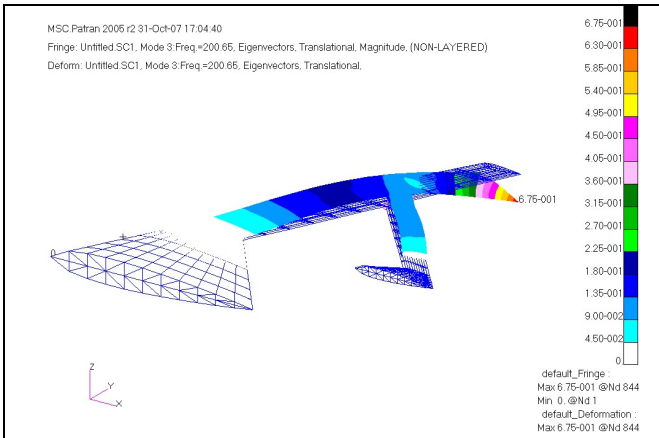

Figure 12 Scaled Sensorcraft model Mode 3 200.6 Hz

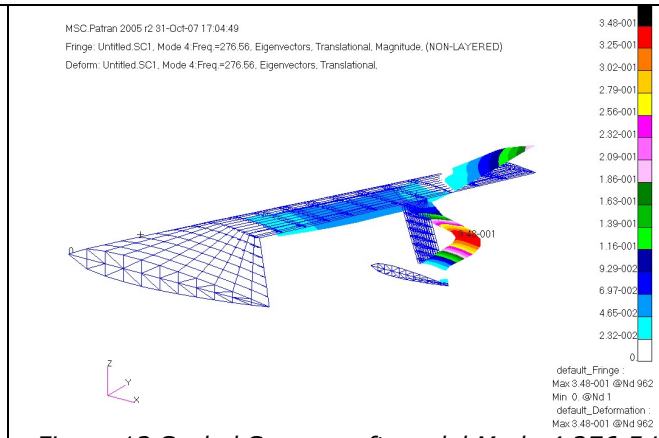

Figure 13 Scaled Sensorcraft model Mode 4 276.5 Hz

6. Matching of Wind Tunnel Scale Model to Full size Model of Sensorcraft

The Sensorcraft Model was divided into 4 sections: Front Fuselage (FF); Rear Fuselage (RF), Front Wing (FW); Rear Wing (RW) with the following construction:

- The front fuselage has a solid plate at mid thickness, 8 ribs and skin.
- The rear fuselage has a solid plate at mid thickness, 8 ribs and skin.
- The front wing has 2 beams located at 25% and 75% chord, 11 ribs and skin.
- The rear wing has 2 beams located at 25% and 75% chord, 9 ribs and skin.
- The beams are of rectangular cross-section and have a constant cross-section throughout the span. The maximum height is dictated by the height of the smallest rib.

The variables for the optimization were:

- FF, RF, FW and RW ribs thickness
- FF and RF block thickness
- FF, RF, FW and RW skin thickness
- FW, RW beams and Fuselage beam section

The objective was to match the first three reduced frequencies (only symmetric modes considered) and static displacement at the leading edge front wing tip. Two models were considered initially: one with skin and ribs on fuselage section as well and a modified version with no ribs or skin over the fuselage section. The cost function utilized was

$$f = W\left[1-\left|M_{FM}-M_{SM}\right| \quad \kappa\left(1-\left|k_{FM}-k_{SM}\right|\right) \quad 1-\left|\delta_{FM}-\delta_{SM}\right|\right]^T$$

$$\kappa = \begin{cases} 1+\dfrac{V_f - V_{MS}}{V_{MS}} & V_f < V_{MS} \\ 1 & V_f > V_{MS} \end{cases} \tag{43}$$

where W is a vector of weighting factors, and κ is a penalty function. M refers to the mass, k to the reduced frequency and δ to the static displacement ratio. The penalty function is introduced to force the flutter speed to be above the Scale Model flight test speed. V_f is the model flutter speed and V_{MS} is the test flight speed.

The subscript FM refers to the Full Scale Model and SM to the Scaled Model. For the following cases the vector W=[0 0.5 0.5]. In table 2, the assigned values to optimisation are listed. Where a number between brackets is present, it corresponds to a different value assigned to the modified model.

Variable	Minimum (m)	Maximum (m)	Divisions (2^n)	Material
FF skin	0.0001	0.001	3	Nylon
RF skin	0.0001	0.001	3	Nylon
FF block	0.0011	0.015	3	Aluminium
RF block	0.0011	0.015	3	Aluminium
WF skin	0.0001	0.001	3	Nylon
WR skin	0.0001	0.001	3	Nylon
WF beam 25% [width height]	0.0011 0.0011	0.015 0.015	3	Aluminium
WF beam 75% [width height]	0.0011 0.0011	0.015 0.015	3	Aluminium
WR beam 25% [width height]	0.0011 0.0011	0.015 0.015	3 (4)	Aluminium
WR beam 75% [width height]	0.0011 0.0011	0.015 0.015	3 (4)	Aluminium
Beam Fuselage [width height]	0.01 0.01	0.03 0.03	3	Aluminium
Ribs	0.0011	0.015	3 (4)	Aluminium

Table 2. Assigned Range of Dimensions for the Optimisation Process

The parameters in table 3 were utilized for the models, noting that the mass is kept as a free parameter. The geometry scaling factor was fixed to 12.

Parameter	Full Scale Model	Model Scale
Mass	1.55365E5 lb	
Span	74.9852 ft	1.5237 m
Airspeed (m/s)	130.41	30
Mach Number	0.39	0.0882
Altitude	5000 ft	0 m
Static Displacement	29.4887 in	

Table 3. Parameters for Optimisation

Material properties of Nylon and Aluminium were fixed as shown in Table 4.

Material	Young's Modulus (N/m^2)	Poisson's Ratio	Density (kg/m^3)
Nylon	$3x10^9$	0.42	1100
Aluminium	$72.9x10^9$	0.33	2700

Table 4. Material Properties

The frequencies of the full scale model at the target airspeed are shown in table 5.

Mode	Frequency (Hz)	Mode	Frequency (Hz)
1	0.7881	11 (Sym)	5.9117
2 (Sym)	1.1307	12	6.0483
3 (Sym)	1.2371	13	6.3137
4	1.3665	14 (Sym)	6.5428
5	2.1782	15	7.7942
6 (Sym)	2.7110	16 (Sym)	7.7455
7	2.5988	17	8.2135
8 (Sym)	3.9146	18 (Sym)	9.4046
9	4.1680	19	9.7755
10 (Sym)	4.6459	20 (Sym)	10.1409

Table 5. Wind-on Modal Frequencies at Target Airspeed

The static calculations were performed with a 5 degree Angle of Attack. The reference length used to calculate the reduced frequency is the span. The optimisation loop was fixed with 33 genes plus 7 new genes for each iteration and 50 generations. Figure 14 shows the convergence for the best 7 genes throughout the generations whereas in figure 15 the best cost is plotted against the history of the elements of the cost function.

Table 6 shows the converged values of the target values for both models.

Parameter	Target value	Achieved value	Achieved value (Modified Model)
Reduced Frequency 1	0.19817	0.20686	0.20516
Reduced Frequency 2	0.21681	0.3494	0.38112
Reduced Frequency 3	0.47513	0.47543	0.47679
Static Displacement Ratio	0.0328	0.042208	0.03142
Mass (kg)	20.88	13.3376	23.755

Table 6. Optimised Parameter Values

Table 7 gives the resulting dimensions of all the elements.

Element	Dimension (m)	Dimensions (m) (Modified Model)
FF skin	0.0001	N/A
RF skin	0.0001	N/A
FF block	0.0011	0.0186
RF block	0.0090	0.0300

WF skin	0.0001	0.0005
WR skin	0.0001	0.0005
WF beam 25% [width height]	0.0051 0.0031	0.0048 0.0020
WF beam 75% [width height]	0.0011 0.0090	0.0011 0.0030
WR beam 25% [width height]	0.0051 0.0130	0.0030 0.0020
WR beam 75% [width height]	0.0011 0.0031	0.0011 0.0048
Beam Fuselage [width height]	0.01 0.01	0.01 0.01
Ribs FF	0.0090 0.0011 0.0130 0.0150 0.0051 0.0011 0.0110 0.0031	N/A
Ribs RF	0.0071 0.0090 0.0130 0.0051 0.0031 0.0130 0.0071 0.0051	N/A
Ribs FW	0.0130 0.0150 0.0150 0.0130 0.0150 0.0090 0.0110 0.0011 0.0031 0.0011 0.0130	0.0137 0.0112 0.0049 0.0124 0.0074 0.0036 0.0137 0.0011 0.0150 0.0175 0.0187 0.0187
Ribs RW	0.0130 0.0130 0.0150 0.0130 0.0130 0.0150 0.0110 0.0071	0.0124 0.0162 0.0162 0.0124 0.0175 0.0200 0.0187 0.0061 0.0036

Table 7. Optimised Dimensions

These results are not as good as expected, particularly in mode 2, however it was subsequently found that there was an error in one of the root boundary conditions. Much better results have now been obtained for the second reduced frequency with this correction in place, with similar results for the other parameters. Little difference was found for the actual internal structural elements for this final case.

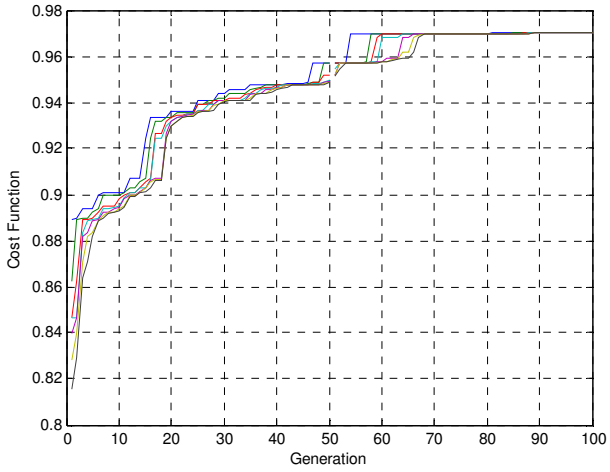

Figure 14. Optimisation evolution

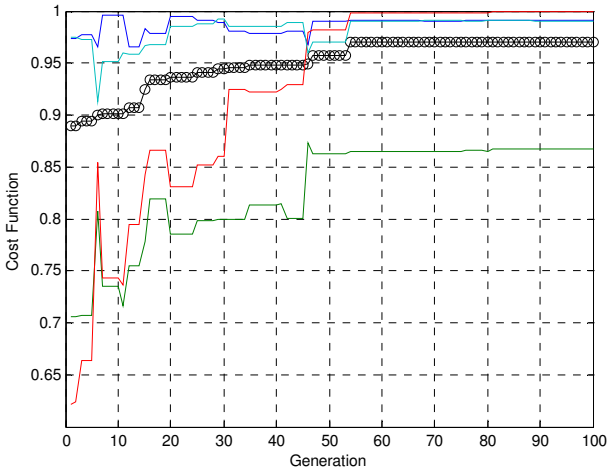

Figure 15. Optimisation cost function. Black line – Best cost function. Blue line – 1st reduced frequency. Green line – 2nd reduced frequency. Red line – 3rd reduced frequency. Cyan line – Static displacement

7. Application of Gust Device to Scaled Sensorcraft Model

7.1 Original Wing

Firstly, the divergence, flutter and gust behaviour of the scaled wing was investigated to provide a baseline for the implementation of the gust device on the sensorcraft. As it is intended to use the model to design a wind-tunnel model and so all aerodynamic analyses was performed using sea-level atmospheric conditions and a velocity of 30m/s.

The divergence speed was found to be 80.846m/s, with bending of the forward wing being the critical mode whereas flutter occurred at 66.373m/s, with the coalescing frequencies associated with mode 1 (rear wing plunge and pitch) and mode 2 (first wing bending of both forward and rear wings).

The gust analysis was performed with a freestream velocity of 30m/s and a '1-cosine' gust was used to provide a standardised discrete input. Part of the FAA airworthiness regulations, the maximum gust that the scaled aircraft should be designed for is 2.957m/s with the specified gust gradient distance (the

distance required for the gust to build to a peak) being 12.5 mean chord lengths of the aircraft. Here, the chord measurement is 0.27356m.

The maximum (absolute) stress encountered during the response (see figure 16) to the gust (which occurs in the rear spar of the forward wing at the root) was found to be 146.361MPa. A peak (absolute) twist of the wing at the tip was found to be 1.6805°. The response was also measured at the point on the span where the wing would be modified; at this point the maximum (absolute) twist encounter was 1.4825° and the maximum (absolute) plunge of the wing (at a point where the wing will be modified to attach the device i.e. 86% span) was 0.050316m.

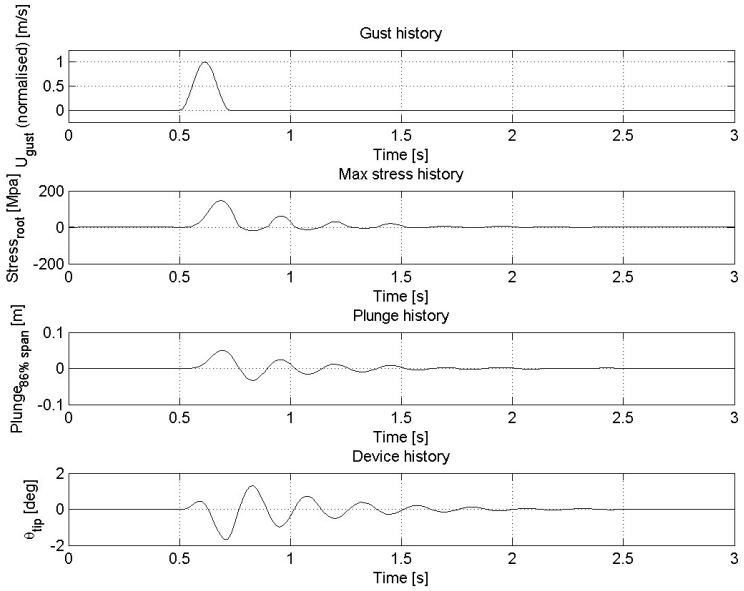

Figure 16. Gust Response for Baseline Wing

7.2 Wing with Gust Alleviation Device

The wing was altered to include a gust-alleviation device. This device replaced part of the outboard section of the wing (86% - 100% span) and was attached to the rest of the wing via a torsional spring close to the leading edge, allowing it to pitch relative to the rest of the wing with an associated stiffness (see figure 17). As the main wing pitches up in response to a gust (and by doing so increasing aerodynamic loads and resultant stresses), the device rotates about the spring (as the aerodynamic centre lies aft of this axis), decreasing its incidence and therefore decreasing aerodynamic loads.

Of interest in this study is the aeroelastic behaviour of the wing when both the stiffness and chordwise position of the attachment are varied. Three attachment points that coincide with existing FE nodes of the model were considered; x/c = 0.0, x/c = 0.08307 and x/c = 0.1666, with c the local chord length and x the chordwise distance from the leading edge (LE).

Figure 18 illustrates the variation of the divergence speed with attachment stiffness for several different chordwise positions of attachment. The critical divergence mode was found to be bending of the forward wing for stiffnesses approximately greater than 50Nm/rad and pitching of the device as well as rear wing bending for stiffnesses below this value. Any worries that the device itself would provide the mechanism for divergence were unfounded.

Although the divergence speed barely alters over the range of stiffnesses considered, the device actually improves the divergence behaviour of the wing slightly; this is due the fact that the attachment points lies ahead of the aerodynamic centre of the device and so a nose-down moment results,

decreasing the angle of incidence of the device as the stiffness decreases. The result is reduced aerodynamic loads on the wing. Furthermore, the plot shows that in terms of divergence behaviour, the closer to the leading edge of the wing the attachment point is, the better; this reflects the greater length of the moment arm between the aerodynamic centre and the axis of rotation. The difference in the divergence speed at high stiffnesses from the original model (80.846m/s) is most likely due to structural modifications to include the device in the FE model. However, the critical modes are identical.

Figure 19 illustrates the modified wing's flutter speed variation with attachment stiffness, for various chordwise attachment points. It is clear that the gust alleviation device has a detrimental effect on the flutter behaviour of the aircraft; as the stiffness of the device decreases, so too does the flutter speed. The significant range of stiffnesses that have a major impact on the flutter speed is between around 5 - 40 Nm/rad. At the upper end of this range a sharp levelling-off of the flutter speed is observed. This effect is caused by a change of modes making the flutter mechanism. Also evident is that the closer the attachment point is to the leading edge, the higher the flutter speed becomes.

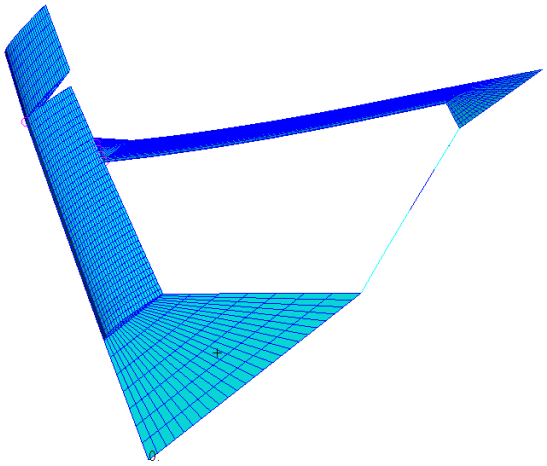

Figure 17. Sensorcraft Model With Gust Alleviation Device

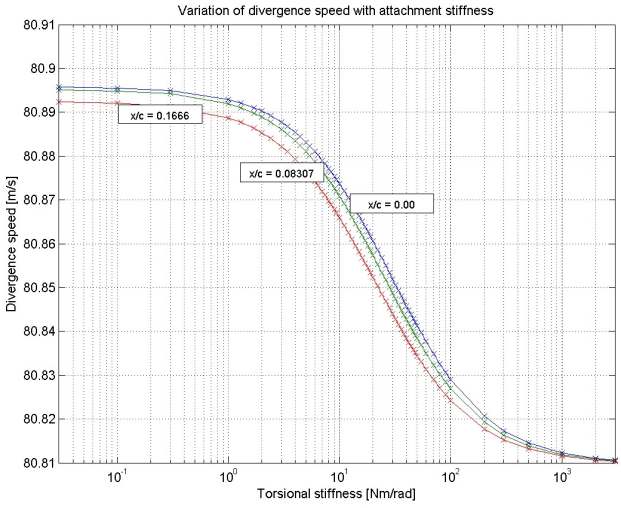

ERROR: undefined
OFFENDING COMMAND: f‘~

STACK: